Coi1 is a novel assembly factor of the yeast complex III–complex IV supercomplex

Ravi K. Singhal[a], Christine Kruse[a], Juliana Heidler[b], Valentina Strecker[b], Klaus Zwicker[c], Lea Düsterwald[d], Benedikt Westermann[e], Johannes M. Herrmann[d], Ilka Wittig[b,f,g], and Doron Rapaport[a,*]

[a]Interfaculty Institute of Biochemistry, University of Tübingen, 72076 Tübingen, Germany; [b]Functional Proteomics, SFB 815 Core Unit, Faculty of Medicine, Goethe University, 60596 Frankfurt am Main, Germany; [c]Institute of Biochemistry I, Faculty of Medicine, Goethe University Frankfurt, 60590 Frankfurt am Main, Germany; [d]Cell Biology, University of Kaiserslautern, 67663 Kaiserslautern, Germany; [e]Cell Biology, University of Bayreuth, 95440 Bayreuth, Germany; [f]Cluster of Excellence "Macromolecular Complexes," Goethe University, 60596 Frankfurt am Main, Germany; [g]German Center of Cardiovascular Research (DZHK), Partner Site RheinMain, 60596 Frankfurt, Germany

ABSTRACT **The yeast bc1 complex (complex III) and cytochrome oxidase (complex IV) are mosaics of core subunits encoded by the mitochondrial genome and additional nuclear-encoded proteins imported from the cytosol. Both complexes build various supramolecular assemblies in the mitochondrial inner membrane. The formation of the individual complexes and their supercomplexes depends on the activity of dedicated assembly factors. We identified a so far uncharacterized mitochondrial protein (open reading frame *YDR381C-A*) as an important assembly factor for complex III, complex IV, and their supercomplexes. Therefore we named this protein Cox interacting (Coi) 1. Deletion of COI1 results in decreased respiratory growth, reduced membrane potential, and hampered respiration, as well as slow fermentative growth at low temperature. In addition, *coi1*Δ cells harbor reduced steady-state levels of subunits of complexes III and IV and of the assembled complexes and supercomplexes. Interaction of Coi1 with respiratory chain subunits seems transient, as it appears to be a stoichiometric subunit neither of complex III nor of complex IV. Collectively this work identifies a novel protein that plays a role in the assembly of the mitochondrial respiratory chain.**

Monitoring Editor
Anne Spang
University of Basel

Received: Feb 6, 2017
Revised: Jul 31, 2017
Accepted: Aug 1, 2017

This article was published online ahead of print in MBoC in Press (http://www.molbiolcell.org/cgi/doi/10.1091/mbc.E17-02-0093) on August 9, 2017.

Author contributions: K.Z., J.M.H., I.W., and D.R. designed the research; R.K.S., C.K., J.H., V.S., B.W., and I.W. performed the research; R.K.S., K.Z., J.M.H., B.W., I.W., and D.R. analyzed the data; and R.K.S. and D.R. wrote the paper.

The authors declare that they have no conflict of interest.

*Address correspondence to: Doron Rapaport (doron.rapaport@uni-tuebingen.de).

Abbreviations used: ABC, ammonium bicarbonate; AGC, automatic gain control; BN, blue native; BSA, bovine serum albumin; Coi1, cytochrome oxidase interacting protein; $DiSC_3(5)$, 3,3′-dipropylthiadicarbocyanine iodide; FDR, false discovery rate; HA, hemagglutinin; IM, inner membrane; IMS, intermembrane space; LC/MS, liquid chromatography/mass spectrometry; LFQ, label-free quantification; MICOS, mitochondrial contact site and cristae organizing system; MOM, mitochondrial outer membrane; ORF, open reading frame; PK, proteinase K; PMSF, phenylmethylsulfonyl fluoride; RCF, respiratory supercomplex factor; ROX, residual oxygen consumption; TCA, trichloroacetic acid; TMS, transmembrane segment.

INTRODUCTION

The mitochondrial inner membrane (IM) is a highly structured compartment that harbors multisubunit respiratory chain complexes. In yeast cells, these complexes are succinate dehydrogenase (complex II), cytochrome bc_1 (complex III), cytochrome *c* oxidase (complex IV), and F_1F_o ATP synthase (complex V). Most of the subunits of the respiratory chain complexes are nuclear encoded and imported from the cytosol into mitochondria. Additional components of the respiratory complexes are encoded by the mitochondrial genome and are synthesized within the organelle. Thus proteins from both origins (nuclear and mitochondrial genome) are assembled into their corresponding complexes within the mitochondrial IM in a coordinated and controlled manner (Barrientos *et al*., 2009; Herrmann *et al*., 2013). The yeast cytochrome oxidase forms a complex that comprises three mitochondrially encoded core subunits and nine components that have to be imported from the cytosol (Geier *et al*., 1995; Soto *et al*., 2012; Levchenko *et al*., 2016; Strecker *et al*., 2016). For their proper enzymatic activity, the respiratory complexes require also cofactors such as heme, copper, zinc, and magnesium, which are

Supplemental Material can be found at:
http://www.molbiolcell.org/content/suppl/2017/08/08/mbc.E17-02-0093v1.DC1

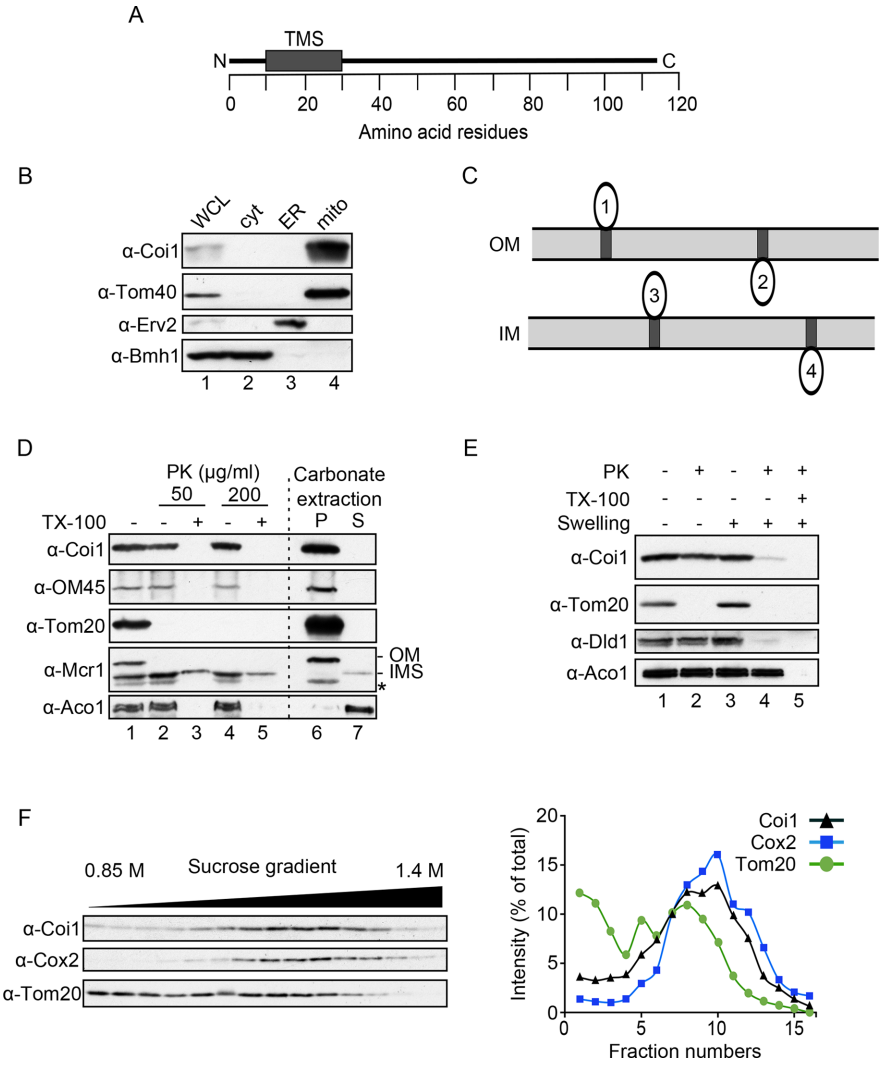

FIGURE 1: Coi1 is a mitochondrial IM protein. (A) Schematic depiction of Coi1. Coi1 is predicted to have a single TMS (aa residues 11–30) that is indicated with a gray box. (B) Coi1 is a mitochondrial protein. Whole-cell lysate (WCL) and fractions corresponding to cytosol (cyt), light microsomal fraction (ER), and mitochondria (mito) were analyzed by SDS–PAGE and immunodecorated with antibodies against Coi1, Tom40 (mitochondrial protein), Erv2 (ER protein), and Bmh1 (cytosolic protein). (C) Schematic representation of the four theoretical possibilities for the membrane topology of Coi1. (D) Coi1 is membrane embedded and protected from external protease. Isolated mitochondria were subjected to externally added PK in the presence or absence of the detergent Triton X-100 (lanes 1–5). Other samples were subjected to alkaline extraction (lanes 6–7). The pellet (P) and the supernatant (S) fractions of the extraction were analyzed by SDS–PAGE and immunoblotting. OM45, OM protein facing toward IMS; Tom20, OM protein exposed toward the cytosol; Mcr1, has two isoforms, a 34-kDa OM form and a 32-kDa IMS form; Aco1, soluble matrix protein; *, degradation product. (E) Coi1 is exposed to the IMS. Isolated mitochondria were left untreated or were swollen before PK was added in the presence or absence of Triton X-100. Samples were analyzed by SDS–PAGE and immunodecoration with antibodies against the indicated proteins. Dld1, an IM protein facing the IMS. (F) Coi1 is an IM protein. Left, isolated mitochondria were subjected to sonication followed by sucrose density gradient centrifugation. Fractions of the gradient were collected and analyzed by SDS–PAGE and immunodecorated with antibodies against the indicated proteins. Right, the intensities of the various bands were quantified and depicted. The sum of all intensities of each protein was set to 100%.

delivered by dedicated factors that are only partially characterized (Horn and Barrientos, 2008; Kim *et al.*, 2012; Soto *et al.*, 2012).

The respiratory complexes are arranged as supercomplexes to facilitate electron transport, to stabilize the individual complexes, and to reduce production of reactive oxygen species (reviewed in Genova and Lenaz, 2014; Greggio *et al.*, 2017). The composition of the various supercomplexes might change depending on cell types and their physiological needs (Genova and Lenaz, 2014; Greggio *et al.*, 2017). In mammalian cells supercomplexes containing complex I, complex III dimer and various copy numbers of complex IV were also named respirasomes (Schägger and Pfeiffer, 2000). In budding yeast cells lacking complex I, supercomplexes consist of a dimer of complex III and one or two copies of complex IV (III_2 + $IV_{1–2}$) (Cruciat *et al.*, 2000; Schägger and Pfeiffer, 2000; Heinemeyer *et al.*, 2007).

The assembly process of the single complexes and the formation of their supercomplexes are mediated by dedicated assembly factors (Mick *et al.*, 2011; Smith *et al.*, 2012; Soto *et al.*, 2012). Recently, two proteins known as respiratory supercomplex factor (RCF) 1 and 2, which directly interact with complex IV and play a role in its stability, were reported (Strogolova *et al.*, 2012; Rydstrom Lundin *et al.*, 2016). Interestingly, even the phospholipid cardiolipin was found to be required for the assembly and stability of supercomplexes (Pfeiffer *et al.*, 2003). However, despite the aforementioned progress, a comprehensive understanding of the assembly process and maintenance of the supercomplexes and a full repertoire of the assembly and regulatory factors are still lacking.

In the current study, we identified and characterized a novel assembly factor that we named cytochrome oxidase interacting protein (Coi) 1 (open reading frame [ORF] *YDR381C-A*). We demonstrate that deletion of Coi1 results in severe alteration in mitochondrial function and hence in growth retardation of yeast cells. The absence of Coi1 resulted in defects in the assembly of complexes III and IV and in the formation of their supercomplexes. Accordingly, we observed physical interactions between Coi1 and subunits of these two complexes. Taken together, our results describe a novel assembly factor of the mitochondrial respiratory chain.

RESULTS

The uncharacterized protein product of ORF *YDR381C-A* was recently found in the interactome of the IM protein Cox4 (Bottinger *et al.*, 2013). This protein was also described to be a part of the proteome of the mitochondrial outer membrane (MOM; Zahedi *et al.*, 2006). In the present study, we aimed to investigate the functional role of this protein in mitochondria. The protein has a molecular mass of 12.7 kDa and lacks homologues in higher eukaryotes. According to in silico prediction, Ydr381c-a has a putative transmembrane segment (TMS) in its N-terminal region (aa residues 11–30) (Quick2D, https://toolkit.tuebingen.mpg.de/#/tools/quick2d) (Figure 1A). Owing to

the molecular interactions with respiratory subunits, as described later, we renamed and will refer to *YDR381C-A* in this report as cytochrome *c* oxidase interacting protein 1 (*COI1*).

Subcellular fractionation of wild-type cells was performed to confirm the reported mitochondrial location of Coi1. The obtained fractions were analyzed by immunoblotting with an antibody raised against Coi1. Similar to the known mitochondrial protein Tom40, Coi1 was enriched in the mitochondrial fraction (Figure 1B). This observation confirms that Coi1 is a mitochondrial protein. Because the protein harbors one putative TMS, four different topologies of the protein with respect to the mitochondrial membranes can be envisaged (Figure 1C).

To address in detail the topology of Coi1 and to verify that the protein is indeed anchored within a membrane, we subjected isolated mitochondria to proteinase K (PK) treatment and to alkaline extraction. Coi1 was present in the membrane fraction of the alkaline extraction, similar to known MOM proteins such as Tom20 and OM45 (Figure 1D, lanes 6 and 7). Proteins exposed on the surface of the organelle (like Tom20 and the OM isoform of Mcr1) were cleaved by PK, whereas the signal of Coi1 was still detectable. On the other hand, Coi1 could not be detected in lysed mitochondria treated with PK, suggesting that Coi1 is PK protected in intact mitochondria (Figure 1D, lanes 1–5). Thus we can exclude topology 1 in Figure 1C.

For further investigation of the orientation of Coi1, mitochondria were swollen in hypo-osmotic condition to disrupt the outer membrane and subsequently treated with PK. This combination eliminated the signal of both Coi1 and the intermembrane space (IMS) protein Dld1. In contrast, the matrix protein aconitase (Aco1) remained protease resistant under these conditions, demonstrating the intactness of the IM (Figure 1E). Considering that the antibody against Coi1 was raised against C-terminal peptides, this outcome suggests that the C-terminus of Coi1 is facing toward the mitochondrial IMS (option 2 or 3 in Figure 1C).

To find out in which membrane Coi1 is embedded, mitochondrial OM and IM vesicles were obtained by hypo-osmotic swelling and sonication. The vesicles were separated by sucrose gradient centrifugation and the collected fractions were analyzed by immunodecoration. Similar to the IM protein Cox2, Coi1 was predominantly detected in heavier fractions. Of note, a minor portion of Coi1 was found in the lighter fractions, resembling the behavior of the OM protein Tom20 (Figure 1F). Hence it might be that Coi1 is partially located at the interface of the inner and the outer membranes. Taken together, these results suggest that Coi1 is embedded in the mitochondrial IM, facing toward the IMS (Figure 1C, topology 3).

Loss of *COI1* causes a severe growth defect on nonfermentable carbon sources

To investigate the function of Coi1 in yeast cells, we deleted the chromosomal copy of *COI1* and analyzed the growth of the deletion strain. Cells lacking Coi1 grew on fermentable carbon source like glucose (yeast extract–peptone–dextrose [YPD]), similar to control cells with a slightly retarded growth on 15°C. In contrast, the *coi1*Δ strain showed severe growth defects on both nonfermentable (YP-glycerol [YPG]) and semifermentable (YP-galactose [YPGal]) carbon sources at all temperatures (Figure 2). Of note, the growth phenotype was more severe at lower temperatures (15 or 24°C) suggesting that the protein's function is especially crucial under these conditions. This growth phenotype is a direct result of the *COI1* deletion, as it could be complemented by reintroduction of either native Coi1 or C-terminally hemagglutinin (HA)-tagged Coi1 (Supplemental Figure S1A). These observations further verify that

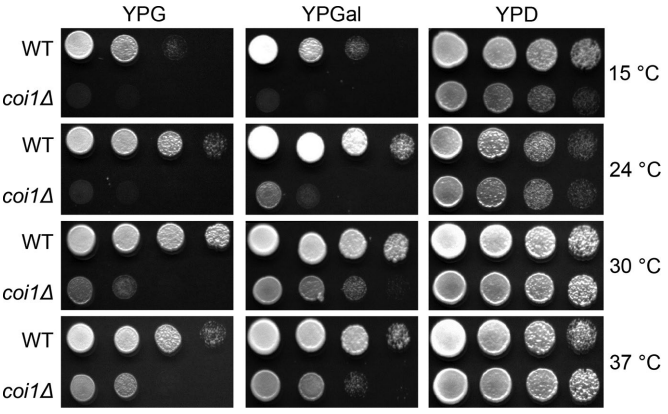

FIGURE 2: Deletion of *COI1* results in a severe growth phenotype. Wild-type (WT) and *coi1*Δ cells were tested by drop-dilution assay at the indicated temperatures on medium containing glycerol (YPG), galactose (YPGal), or glucose (YPD).

ectopically expressed Coi1 and Coi1-HA are functional. Accordingly, Coil-HA was also localized to mitochondria (Supplemental Figure S1B), and, of note, the overexpression in wild-type cells of either native Coi1 or Coi1-HA has no negative effect on the growth condition (Supplemental Figure S1A). Collectively these findings indicate that the loss of Coi1 results in a severe growth defect on nonfermentable carbon sources.

Deletion of *COI1* causes reduction in mitochondrial membrane potential and respiration

The severe growth defect of *coi1*Δ cells on nonfermentable carbon source suggests alterations in mitochondrial functions. Hence we aimed to analyze in detail the performance of mitochondria in the mutated cells. To that end, we measured the membrane potential ($\Delta\Psi$) of isolated mitochondria from wild-type and *coi1*Δ cells with the membrane potential-sensitive dye 3,3′-dipropylthiadicarbocyanine iodide ($DiSC_3(5)$. Quenching of the fluorescence signal was observed immediately upon addition of mitochondria, which was restored by the addition of the ionophore valinomycin. In mitochondria lacking Coi1, the fluorescence quenching was about twofold smaller in comparison to control organelles (Figure 3A). This indicates that Coi1 is required for the optimal function of the respiratory complexes. In line with the reduced $\Delta\Psi$, we also observed impairment in the in vitro import efficiency of the IM proteins Oxa1 and AAC, which require $\Delta\Psi$ for their import (Supplemental Figure S2, A and B). In contrast, the in vitro import of the MOM proteins Tom40 and Porin, which are imported in a $\Delta\Psi$-independent manner, was not affected by the deletion of *COI1* (Supplemental Figure S2, C and D). This suggests that deletion of *COI1* affects the membrane potential and, in turn, indirectly influences the import efficiency of some mitochondrial proteins.

We further analyzed the mitochondrial respiration in the absence of Coi1 by measuring the oxygen consumption in wild-type and *coi1*Δ cells. The whole-cell oxygen consumption was measured by high-resolution respirometry in two steps: the routine respiration was monitored first, and then the maximal uncoupled respiration. Under both conditions, the respiration in *coi1*Δ cells was significantly impaired compared with wild-type cells (Figure 3B). Next the respiration activity of isolated organelles was measured. Mitochondria lacking Coi1 had much lower respiration capacity than control organelles (Figure 3C). Nevertheless, the former organelles had higher respiration ability than the nonrespiring organelles lacking

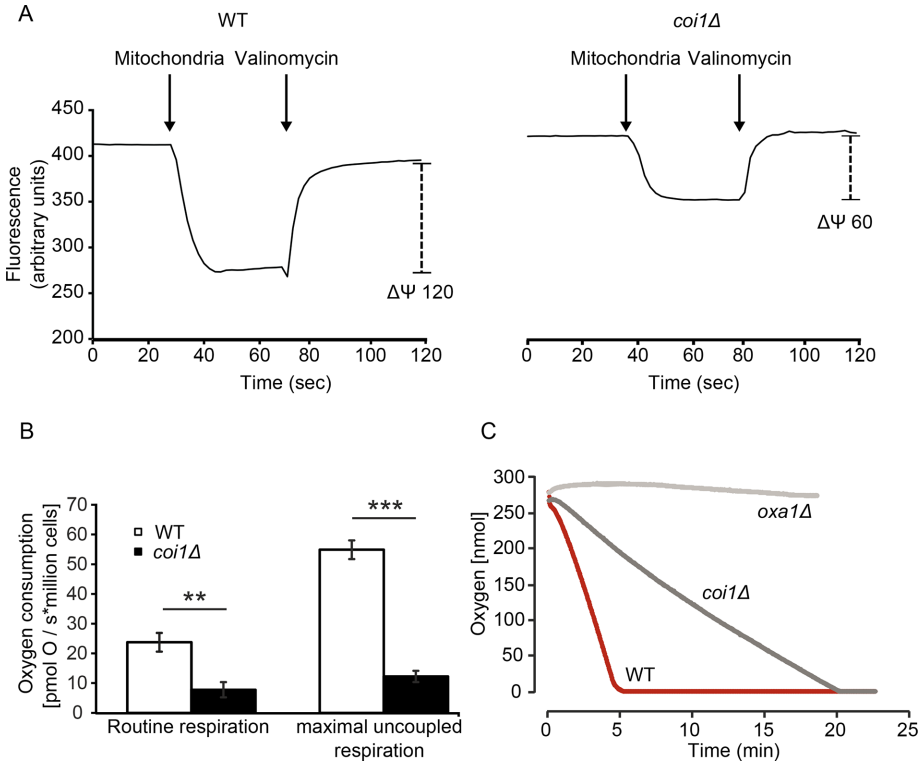

FIGURE 3: Mitochondria lacking Coi1 have lower membrane potential and reduced respiration. (A) Mitochondrial membrane potential is reduced by deletion of *COI1*. ΔΨ of mitochondria isolated from wild-type (WT) or *coi1*Δ cells was monitored by a fluorescence assay with the dye $DiSC_3(5)$. The first arrow indicates the time point of the addition of mitochondria to the dye-containing buffer. The second arrow represents the time point when valinomycin was added to dissipate the membrane potential. The difference in the fluorescence levels before and after the addition of valinomycin is indicated. (B) The oxygen consumption of wild-type and *coi1*Δ cells was analyzed by high-resolution respirometry at 30°C. Error bars indicate SD of three independent experiments. **, $p < 0.01$; ***, $p < 0.001$. (C) Oxygen consumption of mitochondria isolated from wild-type, *coi1*Δ, or *oxa1*Δ cells was measured over time at 24°C.

Oxa1. Taken together, the results demonstrate that Coi1 is required for maintaining optimal mitochondrial respiration activity.

Absence of Coi1 does not affect phospholipid composition or morphology of mitochondria

Alterations in lipid composition of mitochondrial membranes can influence the stability of protein complexes within the organellar membranes. Such compromised stability, in turn, can affect the function of such complexes. To test whether the deletion of *COI1* influences the phospholipid composition of mitochondrial membranes, we isolated mitochondria from wild-type and *coi1*Δ cells grown at 30°C and analyzed their lipid composition by thin-layer chromatography. This analysis did not reveal any observable changes upon the deletion of Coi1 (Supplemental Figure S3).

To investigate further the function of Coi1, we studied the mitochondrial morphology in *coi1*Δ cells. To that end, cells expressing a mitochondrial targeted green fluorescent protein (GFP) were grown at 30°C and analyzed by fluorescence microscopy. We did not observe any alterations in the organellar morphology in cells lacking Coi1 (Supplemental Figure S4, A and B). Along this line, the ultrastructure of mitochondria, i.e. morphology and amount of cristae, was not altered upon deletion of *COI1* (Supplemental Figure S4C). Collectively it appears that Coi1 does not play a role in maintaining mitochondrial phospholipid profile or in establishing the organellar morphology.

The steady-state levels of a subset of mitochondrial proteins are reduced in *coi1*Δ cells

The reduced in vitro import of IM proteins and the hampered respiration led us to compare the steady-state levels of proteins in mitochondria isolated from *coi1*Δ cells to those in control organelles. The steady-state levels of components of respiratory complexes such as Cox2, Qcr6, and Cyb2 were reduced in the mutant organelles. In addition, the levels of the matrix protein aconitase (Aco1) and of carrier proteins such as AAC and Pic2 were also affected (Figure 4, A and B). In contrast, the levels of other IM proteins like Oxa1 and Cox4 or of a matrix protein like Hsp70 were not affected (Figure 4, A and B). Similarly, MOM proteins were hardly affected or were observed in slightly reduced amounts (Figure 4, C and D). Of note, the translation capacity of mitochondria lacking Coi1 as compared with that of control organelles was similar or only marginally reduced when cells were grown on galactose or glucose, respectively (Supplemental Figure S5). We therefore conclude that the absence of Coi1 results in lower levels of some mitochondrial proteins like components of the respiratory chain complexes III and IV, and this reduction cannot be explained by hampered mitochondrial translation.

Coi1 physically interacts with subunits of complexes III and IV

Our aforementioned results demonstrate that the absence of Coi1 affects respiration activity and the levels of some respiratory components. To better understand the involvement of Coi1 in respiration, we searched for its interaction partners. To identify such partners, we generated a yeast strain expressing C-terminally HA-tagged Coi1. This tagged version is functional and acquired the correct mitochondrial location (Supplemental Figure S1, A and B). Next we isolated mitochondria from this strain, solubilized the organelles with Triton X-100, and performed affinity purification. Various components of complex III (Cor1, Qcr6), complex IV (Cox2, Cox4), the carrier protein Pic2, and the contact site protein, Mic60 coeluted with Coi1-HA (Figure 5A). These interactions with Coi1 are specific, as they were not observed in the control strain. Furthermore, other mitochondrial proteins such as the soluble matrix protein Aco1, the IM protein Tim23, complex V protein Tim11, and the OM protein Tom22 were not coeluted with Coi1-HA (Figure 5A, bottom). These findings demonstrate that Coi1 physically interacts with components of complexes III and IV.

Interestingly, the mitochondrial contact site and cristae organizing system (MICOS) central subunit Mic60 was also coeluted with Coi1-HA. Therefore we asked whether the physical interactions of Coi1 require the presence of Mic60. To address this issue, we expressed Coi1-HA in a strain lacking Mic60 and performed affinity purification similar to that described earlier. We observed that the interactions between Coi1-HA and its partners were considerably reduced in the absence of Mic60 (Figure 5B). Interestingly, the HA-tagged form of Coi1 also pulled down the native form of the

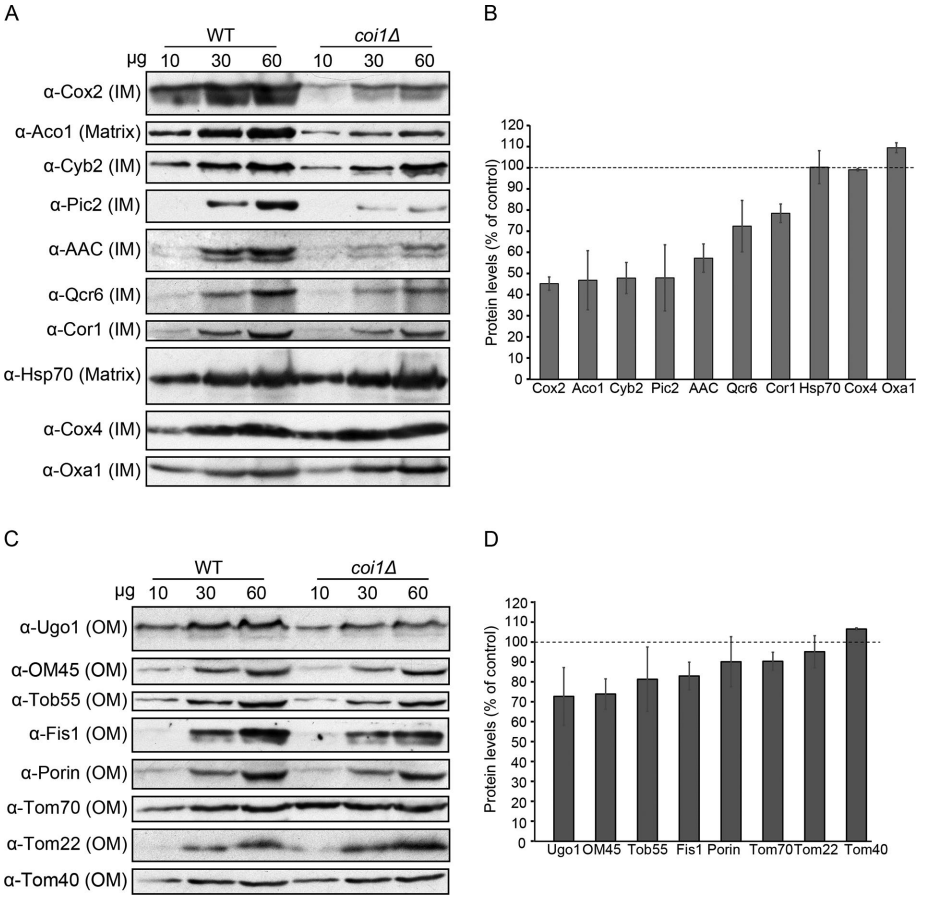

FIGURE 4: Deletion of *COI1* affects the steady-state levels of mitochondrial proteins. (A, C) The indicated amounts of mitochondria isolated from either wild-type (WT) or *coi1*Δ cells were analyzed by SDS–PAGE and immunodecoration with the indicated antibodies. (B, D) The intensity of the bands from three independent experiments such as those presented in A and C was monitored, and the amounts of proteins in mitochondria lacking Coi1 are presented as mean percentages of their levels in control organelles. Error bars represent ±SD.

protein, suggesting that the functional unit of Coi1 contains at least two copies of the protein. This interaction was also reduced in the absence of Mic60. Collectively it appears that Mic60 is stabilizing, directly or indirectly, the interactions of Coi1 with its partners.

Considering this effect of Mic60, we wondered how the absence of other subunits of the MICOS complex would influence the association of Coi1 with its interaction partners. To that end, we performed the pull-down experiments with Coi1-HA using mitochondria lacking Mic10, Mic19, or Mic27. Surprisingly, the absence of either Mic19 or Mic27 resulted in a stronger interaction of Coi1 with respiratory components such as Cox2, Cox4, and Cor1 or with the MICOS subunit Mic10. On the other hand, the amounts of eluted Pic2 were decreased upon deletion of Mic19 or Mic27. Deletion of Mic10 did not have major influence on the interactions of Coi1 (Supplemental Figure S6). These observations suggest that the various MICOS subcomplexes can modulate the interactions of Coi1 with respiratory components. Interestingly, more Tom40 molecules were associated with Coi1 in all deletion strains (Supplemental Figure S6). A possible explanation for this observation is the accumulation of more import intermediates in these mutated organelles.

To obtain a more comprehensive picture on the interactome of Coi1, we used mass spectrometry (MS) to analyze proteins bound to Coi1-HA. For clear presentation of the level of significance and fold changes (as compared with control samples), we present our data as a volcano plot. The plot shown in Figure 6 presents the ratio of a signal for a certain protein in the eluate of a strain harboring HA-tagged Coi1 as compared with a background signal in the eluate of the control strain. Thus the most significant hits with the highest binding are in the upper right zone of the plot. This analysis verifies that components of complexes III and IV such as Qcr1, Qcr2, Cox2, and Rcf1 are highly enriched in the group of strong interactors of Coi1 (Figure 6 and data set in the Supplemental Material). Of note, the significant enrichment of assembly factors of complex III (Cbp2) and complex IV (Shy1) suggest that Coi1 may play a role in the biogenesis of respiratory chain complexes and supercomplexes. In agreement with the results in Figure 5, the central component of the TOM complex, Tom40, also appears to interact with Coi1-HA. However, we propose that this interaction occurs when newly synthesized molecules of Coi1-HA are on their way to be imported into the IM.

Coi1 plays an important role in the formation and stability of respiratory supercomplexes

Our results so far suggest a strong physical and functional link between Coi1 and complexes III and IV. Thus we next asked whether Coi1 is required for assembly and/or stability of these complexes. To address this question, we analyzed respiratory complexes from wild-type and *coi1*Δ cells by blue native (BN)-PAGE and Coomassie staining. Of note, reduced levels of complex IV and its supercomplexes with complex III were observed in cells lacking Coi1 (Figure 7A). To verify the defect in complex IV, we performed a specific heme staining. In the absence of Coi1, complex IV in its monomeric form or as part of its supercomplexes had almost no heme staining, pointing to an impaired complex IV assembly or heme integration (Figure 7B).

To substantiate these conclusions, we further monitored the complexes by Western blotting. Immunodecoration with antibodies against a subunit of complex IV (Cox26) and of complex III (Rip1) indicated alterations in these complexes upon deletion of Coi1 (Figure 7, C and D). Cox26 was detected in two weak bands ($Int1_{cox}$ and $Int2_{cox}$) in the migration range of monomeric complex IV, and a size shift was observed for the supercomplexes. In addition to the size shift, considerably fewer supercomplexes III/IV were detected (Figure 7C). These observations indicate assembly problems in the absence of Coi1 that are manifested as an altered composition or a dead-end assembly intermediate. We also analyzed complex III by immunodecoration with antibodies against Rip1. Similar to the results with complex IV, we observed an assembly defect of complex III in the absence of Coi1 (Figure 7D). Deletion of *COI1* resulted in lower abundance of complex III dimers ($Int3_{bc1}$) and of supercomplexes III/IV and a shift in their migration behavior. In line with a reduced assembly, we detected increased accumulation of Rip1 monomer in the absence of Coi1 (Figure 7D).

Owing to the physical interactions with components of complex IV, we wondered whether Coi1 is a stoichiometric subunit of this

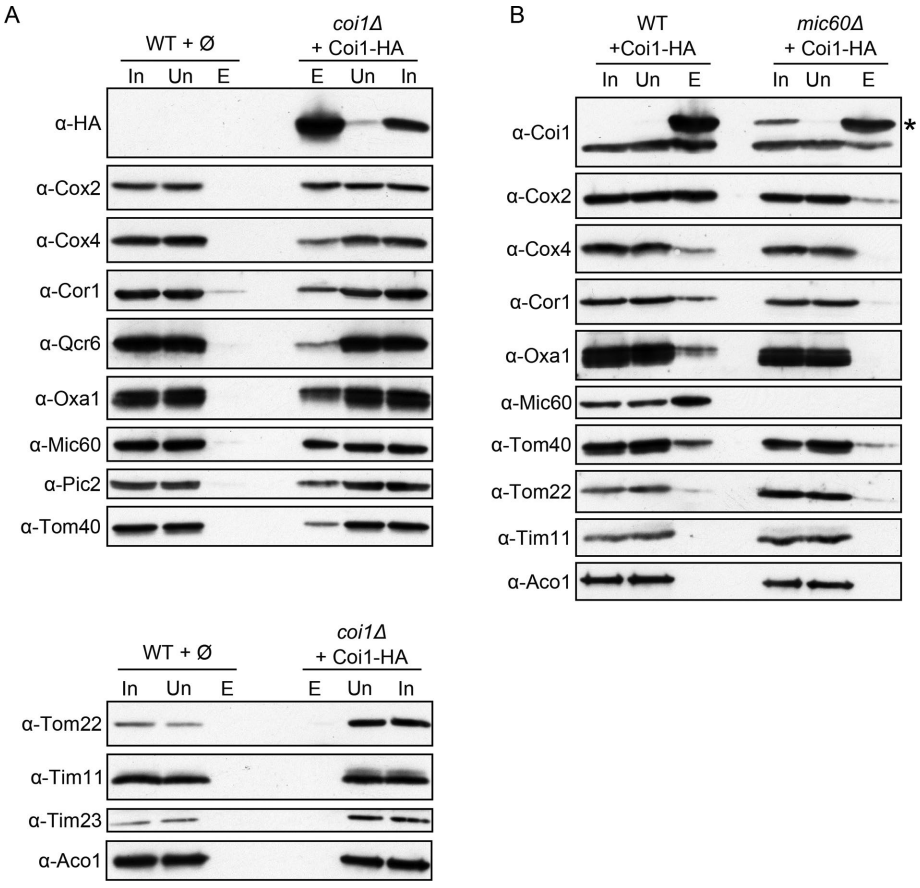

FIGURE 5: Coi1 interacts with components of complexes III and IV. (A) Mitochondria were isolated from either wild-type (WT) or *coi1*Δ cells expressing Coi1-HA. The organelles were lysed with buffer containing Triton X-100, and after a clarifying spin, the supernatants were subjected to pull-down with anti-HA beads. Supernatant (In, 2% of total), unbound material (Un, 2% of total), and the eluates (E, 33.3% of total) were analyzed by SDS–PAGE and immunodecoration with the indicated antibodies. (B) Mitochondria were isolated from wild-type and *mic60*Δ cells expressing Coi1-HA. Further treatment and analysis were as described for A. The HA-tagged form of Coi1 is indicated with an asterisk.

complex. To that end, we analyzed Coi1-containing hetero-oligomeric structures by BN-PAGE followed by immunodecoration. The majority of the Coi1 signal was detected in the low-molecular-mass range (20–250 kDa), whereas only a small portion of the Coi1 molecules were detected in a complex of approximately 1000 kDa. Importantly, this high-molecular-mass complex was also detected in control cells by the anti-Cox2 antibody (Figure 7, E and F). To verify that a subpopulation of Coi1 is indeed associated with complex IV, we also analyzed Coi1 and complex IV in strains deleted for Cox subunits. As expected, Cox2 was observed in these mutated samples in a smaller intermediate species. Notably, Coi1 was also detected to be part of these assembly intermediates (Figure 7, E and F). Hence Coi1 appears not to be a stoichiometric subunit of complex IV but rather to transiently interact with it.

Accumulation of assembly intermediates in organelles lacking Coi1 was further substantiated upon analyzing the complexome of mitochondria isolated from either wild-type or *coi1*Δ cells. Mitochondrial proteins were solubilized in digitonin, and the various respiratory complexes were separated by BN-PAGE and subsequently serially analyzed by MS (Figure 8). Many more assembly intermediates of complex IV were detected in the mutated mitochondria. In addition, organelles lacking Coi1 contained fewer high-molecular-mass supercomplexes (>1000 kDa) that harbored components of both complexes III and IV. Of note, no major changes in the migration of components of complex V were observed in mitochondria isolated from *coi1*Δ cells (Figure 8), suggesting a rather specific effect on complexes III and IV. The complexome analysis verified that Coi1 is not an integral component of the respiratory complexes.

The reduced assembly of complex IV led us to also test whether its enzymatic activity is altered in cells lacking Coi1. We observed a major reduction in the activity of complex IV, whereas the activity of the citrate synthase, which was monitored as a control, was reduced only slightly and in a nonsignificant manner (Figure 9A). To better understand the alterations in the respiratory complexes upon the deletion of Coi1, we compared the heme-absorbance spectra in organelles isolated from *coi1*Δ cells with those from control organelles. Of note, heme A absorption, which is typical for complex IV, appeared with decreased intensity in the mutated organelles, whereas heme B and heme C absorption was hardly affected (Figure 9B). Collectively the heme-staining results and the heme-absorbance measurements suggest that Coi1 is required for the proper transfer of heme A to complex IV and/or its assembly into this complex.

The aforementioned results strongly support a role of Coi1 in assembly of the respiratory supercomplexes. To substantiate such a role, we monitored the assembly of newly synthesized subunits into their corresponding complexes by employing in organello assays. First, we monitored the assembly of newly synthesized mitochondrially encoded Cox2 molecules. Both the monomeric form of Cox2 and assembled species could be detected in control organelles after 30 min of translation. Of note, immunodetection of the steady-state molecules identified only assembled molecules (Supplemental Figure S7). In contrast, in mitochondria lacking Coi1, the newly synthesized molecules were detected almost exclusively as monomeric species, and the steady-state species were observed as a mixture of assembled, intermediate, and monomeric forms (Supplemental Figure S7). The hampered assembly in organelles lacking Coi1 resembles the situation in mitochondria deleted for the known assembly factor Shy1 (Supplemental Figure S7).

Assembly defects were also observed with nuclear-encoded respiratory subunits. Radiolabeled molecules of either Cox13 or Rcf1 were incubated in vitro with mitochondria isolated from either wild-type or *coi1*Δ cells. Organelles lacking the established assembly factor Rcf1 were also included for comparison. Organelles lacking either Coi1 or Rcf1 showed reduced capacity to assemble the newly synthesized molecules into pre-existing supercomplexes III_2IV_2 (Supplemental Figure S8). Thus our findings indicate that Coi1 is required for optimal assembly in organello of either mitochondria- or nuclear-encoded respiratory components.

Finally, we compared the growth phenotype of *coi1*Δ cells with those of cells lacking subunits of complex IV, like Cox6, Cox11, and

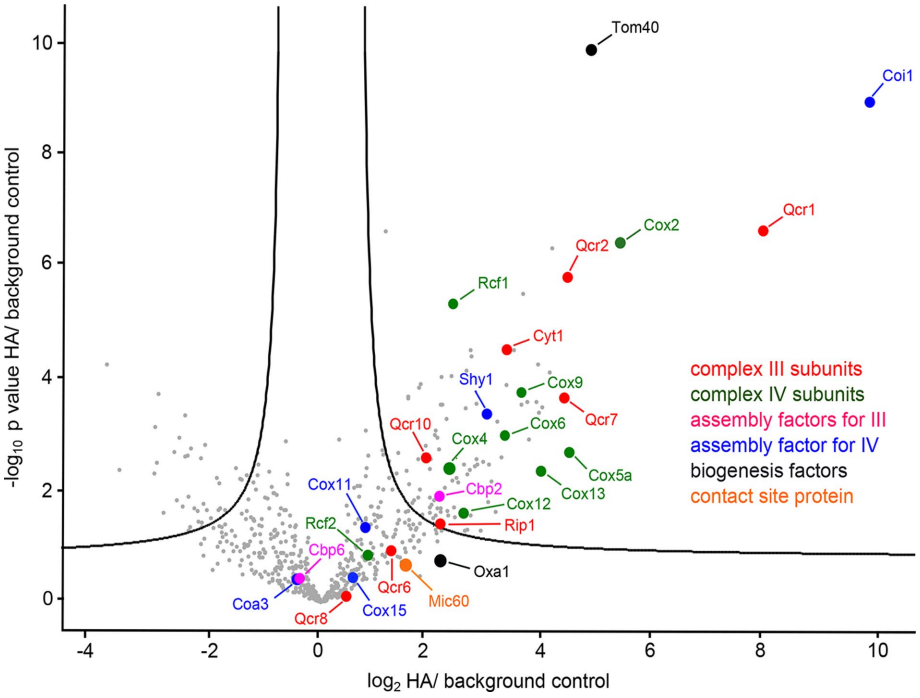

FIGURE 6: Interaction partners of Coi1. Isolated mitochondria from cells described in the legend to Figure 5A were solubilized with Triton X-100 and subjected to affinity purification with anti-HA beads. Eluted fractions were treated with trypsin and analyzed by quantitative MS. The $\log_2$ fold change (*x*-axis) and the negative $\log_{10}$ *p* value (*y*-axis) of protein hits from the organelles harboring Coi1-HA as compared with control organelles from six independent experiments were determined and plotted. Proteins belonging to the same complex are shown in the same color; complex III subunits in red, complex IV subunits in green, assembly factors of complex III in pink, assembly factors of complex IV in blue, and biogenesis factors in black.

Cox19. Interestingly, the absence of Coi1 at lower temperatures (15 or 24°C) results in a slightly more severe growth retardation as compared with the other deletion strains. In contrast, at normal (30°C) or elevated (37°C) temperature, the *coi1*Δ cells grew better than the other mutants did on nonfermentable (YPG) or semifermentable (YPGal) carbon source (Supplemental Figure S9). This outcome suggests again that Coi1 does not behave as a typical core subunit of complex IV and its function is especially important at lower temperatures.

The CXXXH motif of Coi1 is not crucial for its stability or function

To further investigate the relevance of Coi1 for heme assembly, we screened the amino acid sequence of Coi1 for possible heme-binding motifs. Heme-binding domains usually consist of the motif CXXCH, but it was also reported that the motifs CXXXH or XXCH, lacking one of the two cysteines of the canonical motif, can still lead to a transient interaction with heme (Allen *et al.*, 2004; Mavridou *et al.*, 2012). Interestingly, the CXXXH motif was identified in residues 77–81 of Coi1. To investigate the role of these amino acids in the function of Coi1, we constructed variants harboring single point mutations replacing either Cys-77 by serine (C77S) or His-81 by alanine (H81A) and double replacement (Supplemental Figure S10A). These mutated Coi1 versions were expressed in yeast cells lacking the native protein. The steady-state levels of the Coi1 variants were analyzed, and all of them were detected in levels similar to the native protein (Supplemental Figure S10B). Thus these mutations did not affect the stability of Coi1. Next the rescue capacities of the different Coi1 variants were monitored by a drop-dilution assay. All variants could rescue the growth phenotype of *coi1*Δ cells to an extent similar to that of the native protein (Supplemental Figure S10C). This similar growth suggests that the putative heme-binding domain in Coi1 does not play a major role in the function of the protein.

The transmembrane domain of Coi1 is crucial for its function

We next turned to an investigation of the importance of various regions of Coi1 for its overall function. Coi1 has a single putative TMS of 20 amino acids toward its N-terminus region (aa 11–30), and it does not have a canonical presequence (Figure 1A). To understand the importance of the N-terminal region, we generated two N-terminal truncated versions of Coi1 lacking either amino acids 2–9 (Coi1-Δ2-9) or 2–30 (Coi1-Δ2-30). Next the mutated variants were ectopically expressed in *coi1*Δ cells, and a complementation assay was performed. Whereas Coi1-Δ2-9 showed almost native-like complementation capacity, the *coi1*Δ growth phenotype could not be rescued by Coi1-Δ2-30 (Supplemental Figure S11A). In agreement with the slightly reduced functionality, the steady-state levels of Coi1-Δ2-9 were somewhat reduced in both whole-cell lysate and mitochondrial fraction in comparison to overexpressed full-length Coi1. The Coi1-Δ2-30 variant was not detected at all, suggesting that loss of the putative TMS probably leads to mistargeting of the protein and rapid degradation of the truncated version (Supplemental Figure S11B).

To test whether Coi1-Δ2-9 is embedded in the membrane, we performed alkaline extraction. Coi1-Δ2-9 was inserted into the membrane similarly to native Coi1 and the MOM protein Tom40 (Supplemental Figure S11C). These findings indicate that residues 2–9 of Coi1 have only a marginal effect on the stability and function of the protein, whereas residues 11–30 appear to be crucial for the stability of the protein and its correct mitochondrial targeting.

Conserved residues at the C-terminal domain of Coi1 have a functional role

Coi1 has homologues in many fungi, and it contains several conserved, positively charged amino acids at its C-terminal region (Figure 10A). To determine the role of these amino acids, we generated different C-terminal truncations of Coi1 and performed a complementation assay. Truncated versions of Coi1 lacking amino acids 85–114 (Coi1-Δ85-114), 88–114 (Coi1-Δ88-114), 99–114 (Coi1-Δ99-114), 103–114 (Coi1-Δ103-114), or 109–114 (Coi1-Δ109-114) were constructed (Figure 10A). Next these variants were ectopically expressed in *coi1*Δ cells, and their capacity to rescue the growth phenotype of these mutated cells was examined. Coi1-Δ103-114 and Coi1-Δ109-114 showed a partial rescue capacity, whereas the other deletion variants lacked such capability (Figure 10B). As a positive control, full-length Coi1 was able to rescue the *coi1*Δ phenotype (Figure 10B and Supplemental Figure S1).

Obviously, lack of complementation capacity can result from low expression level of these variants. For testing the steady-state levels

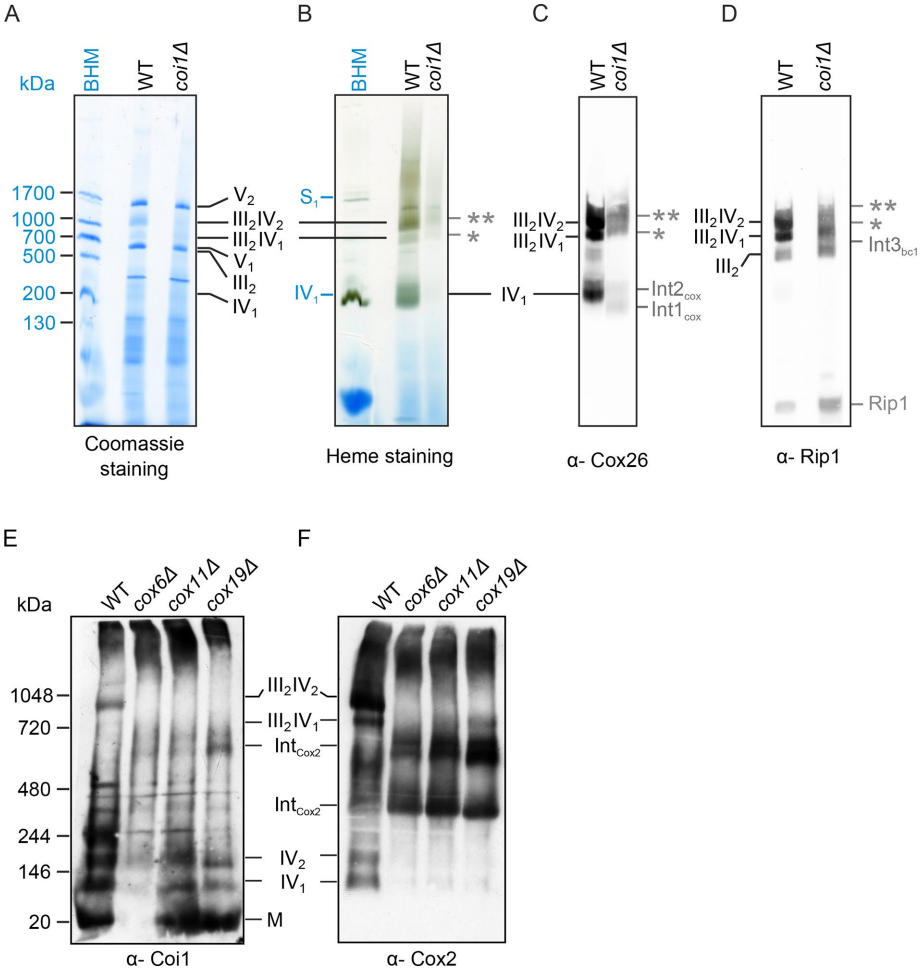

FIGURE 7: Coi1 is essential for assembly of complexes III and IV and their supercomplexes. (A) Mitochondria isolated from either wild-type (WT) or *coi1*Δ cells were analyzed by BN-PAGE. Samples were solubilized using digitonin (final concentration 2.5% [wt/vol]), and the gels were stained with Coomassie. (B) Samples were analyzed as in A, and the cytochrome oxidase complex was detected by specific heme staining. (C, D) Samples were analyzed as in A and then immunodecorated with antibodies against the complex IV subunit Cox26 (C) or the complex III component Rip1 (D). Black annotations describe yeast complexes, and blue annotations indicate complexes from bovine heart mitochondria (BHM) as mass ladder. Complexes and proteins marked in gray highlight the altered appearance of supercomplexes III_2IV_1 (*), III_2IV_2 (**), Rieske protein of complex III (Rip1), complex IV and its assembly intermediates ($Int1_{cox}$, $Int2_{cox}$), and complex III and its assembly intermediate ($Int3_{bc1}$). Assignment of mitochondrial complexes: V_1 and V_2, monomeric and dimeric ATP synthase; III_2, dimeric complex III; IV_1, monomeric complex IV; III_2IV_1, supercomplex containing complex III dimer and one copy of complex IV; III_2IV_2, supercomplex with two copies of each complex III and complex IV; S1, mammalian supercomplex containing complex I, two copies of complex III, and one copy of complex IV. (E, F) Mitochondria isolated from the indicated strains were analyzed by BN-PAGE and then immunodecorated with antibodies against either Coi1 (E) or Cox2 (F).

of the various Coi1 forms, mitochondria were isolated, and the levels of the truncated Coi1 versions were compared with those of plasmid-encoded full-length Coi1. The steady-state levels of Coi1-Δ103-114 and Coi1-Δ99-114 were only slightly reduced compared with the native protein, and the levels of Coi1-Δ109-114 were moderately reduced. Of note, using the anti-Coi1 antibody, no signal could be detected for the truncated versions Coi1-Δ85-114 and Coi1-Δ88-114. The similar levels of Hsp70 and Tom40 in all lanes exclude unequal loading as a cause for the lack of detection (Figure 10C). The Coi1 antibody was raised against a mixture of two C-terminal peptides (corresponding to amino acid residues 81–100 and 101–114). Therefore the inability to detect the latter versions probably results from the absence of the appropriate epitopes in these proteins.

To verify this point, we tagged the truncated versions of Coi1 with HA. These constructs were ectopically expressed in *coi1*Δ cells, and a complementation assay was performed. In this case, the growth phenotype of *coi1*Δ cells was partially rescued only by the Coi1-Δ109-114 variant, while it was not rescued by the other four variants (Supplemental Figure S12A). These findings indicate that the HA-tag has a negative effect on the function of the protein. The steady-state levels of the HA-tagged proteins were also tested in these strains, and interestingly, the anti-HA immunodecoration showed that all the truncated versions of Coi1-HA were expressed to the same levels as the full-length Coi1-HA (Supplemental Figure S12B). This suggests that the truncation of the different segments at the C-terminal region does not affect the expression levels or the stability of the protein. This, in turn, indicates that the reduced signal observed with the Coi1 antibody is indeed due to the loss of the epitopes in the shorter variants. We further confirmed that all the truncated variants were correctly integrated into the IM, as verified by alkaline extraction (Supplemental Figure S12C). Therefore the inability of the truncated variants to complement the growth phenotype is not due to different protein levels or wrong topology but rather due to altered functionality.

Next we wondered whether the lack of activity of certain C-terminally truncated variants is correlated with a reduction in their capacity to maintain interactions with other proteins. To that end, we monitored the ability of HA-tagged Coi1 and two of its truncated variants to pull down other mitochondrial proteins. Interestingly, the two truncated forms interact more tightly with the import component Tom40 (Supplemental Figure S13A), raising the possibility that their import is slowed down compared with the native protein. Of note, whereas the removal of the last six residues did not affect the capacity of Coi1 to interact with components of the respiratory complexes like Cox2 and Cor1, a variant lacking the last 16 residues had a reduced capacity to interact with these proteins (Supplemental Figure S13A). This difference between the two variants nicely correlates with the elevated capacity of Coi1-Δ109-114 to rescue the *coi1*Δ growth phenotype (Figure 10B). Along the same line, we observed altered assembly of respiratory components like Cox26 or Rip1 into respiratory supercomplexes in the strain expressing the Coi1-Δ99-114 variant (Supplemental Figure S13B). Strains containing this truncated variant harbor fewer III_2IV_2 or

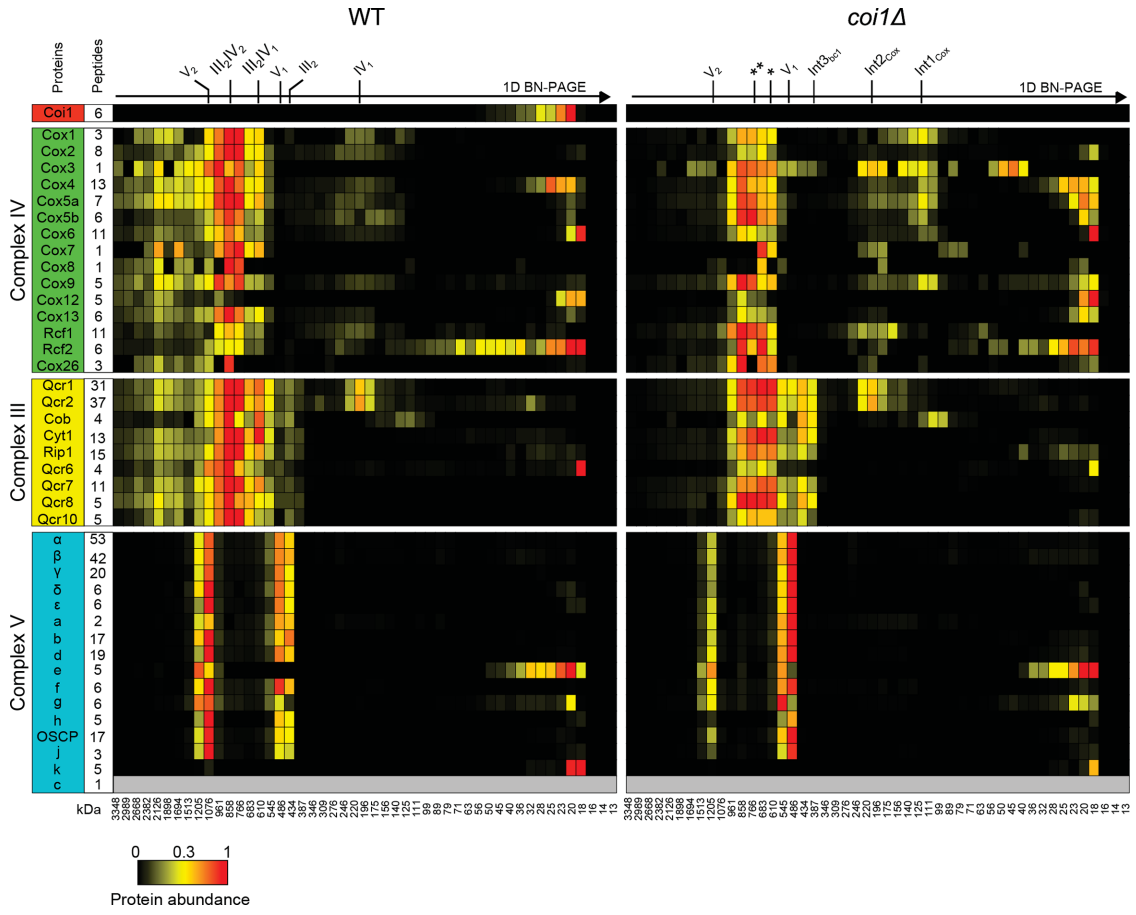

FIGURE 8: Complexome profiling of mitochondria isolated from either wild-type (WT) or Δ*coi1* cells. Mitochondria were isolated from either WT or Δ*coi1* cells and then solubilized with digitonin. Proteins were separated by BN-PAGE, and the gel lane was cut into 50 gel slices of equal size. The protein content of each slice was analyzed by MS. The quantitative information on the abundance of proteins in each slice was then used to create migration profiles for the indicated proteins. For easier visual inspection, the data matrices are displayed as a heat map. Proteins are sorted into their corresponding respiratory complexes. Coi1 distribution is depicted in the top row. Abbreviations are defined in the Figure 7 caption.

III_2IV_1 supercomplexes and elevated amounts of complex III dimer (III_2). Taken together, the positively charged amino acids at the C-terminal region of Coi1 are important for its interaction with respiratory components and its effect on respiratory complexes.

In summary, our findings identify Coi1 as a novel protein of the mitochondrial IM that is critical for the assembly of complexes III and IV and formation of their supercomplexes. The TMS of the protein and conserved regions in the C-terminal domain are essential for the functionality of Coi1.

DISCUSSION

The mitochondrial respiratory chain complexes are arranged in series of intricate structures. These multifaceted structures are assembled by an array of factors bringing the complexes together to a working state. In the current study, we identified a novel protein Coi1 that is conserved in fungi but has no apparent homologues in higher eukaryotes.

Cells lacking Coi1 contain mitochondria with hampered functions

The deletion of *COI1* results in cell growth retardation, dissipation of the mitochondrial membrane potential, and defects in oxidative phosphorylation activity. On the other hand, Coi1 does not seem to be involved in establishing the phospholipid composition of mitochondrial membranes or in the organelle's morphology. Furthermore, the absence of Coi1 causes also major reduction in the amounts of heme associated with complex IV. In line with these phenotypes, Coi1 interacts with various components and assembly factors of the respiratory chain complexes III and IV and with MICOS components. These findings are in line with a previous study in which Coi1 was found to be part of the interactome of Cox4 (Bottinger *et al.*, 2013). Considering these observations, Coi1 resembles Rcf1 and 2, which mediate supramolecular interactions between complexes III and IV (Strogolova *et al.*, 2012), and like Rcf2, Coi1 occurs only in fungi.

The observed interactions of Coi1 with MICOS subunits are in agreement with a recent report that MICOS coordinates its function with respiratory complexes (Friedman *et al.*, 2015). Of note, we observed weaker interactions of Coi1 with the subunits of the respiratory complexes in the absence of Mic60 but stronger ones in the absence of either Mic19 or Mic27. A potential explanation for these various effects would be that different substructures of the MICOS complex modulate the positioning of the respiratory complexes and Coi1 in a dynamic manner and thus regulate their interactions. In line with our findings, recent studies have shown that the MICOS complex is required for efficient function of respiratory chain complexes in both yeast and mice (Cogliati *et al.*, 2013; Friedman *et al.*, 2015).

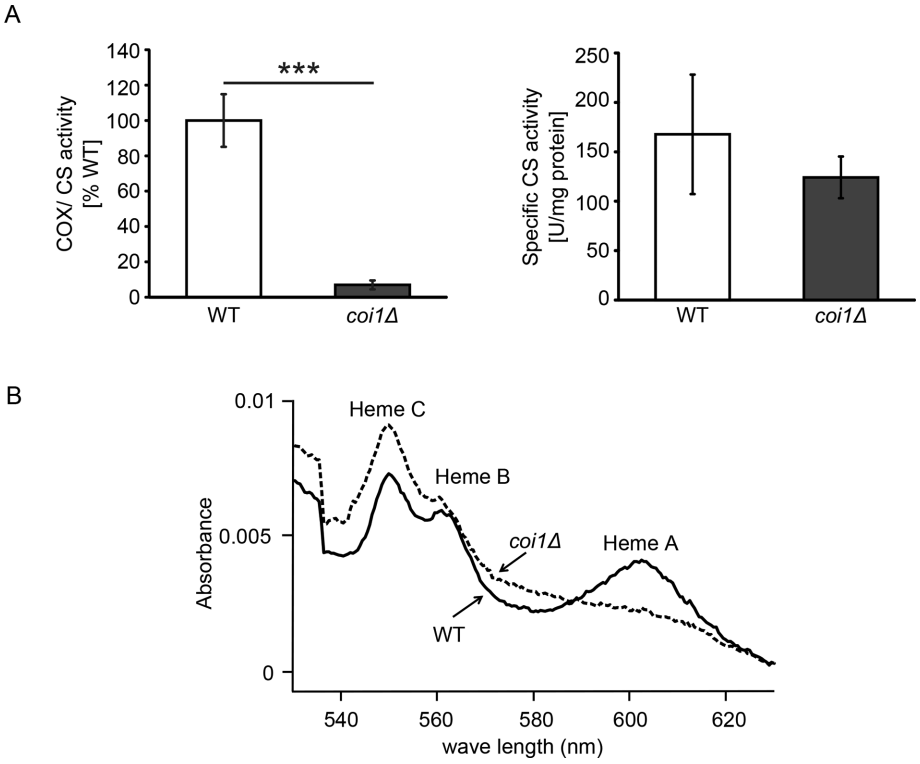

FIGURE 9: Cells lacking Coi1 have reduced cytochrome *c* oxidase activity and altered heme absorbance. (A) Enzymatic activity of cytochrome *c* oxidase (COX) and citrate synthase (CS) were analyzed at 30°C in isolated mitochondria from either wild-type (WT) or *coi1*Δ cells. Left, Cox activity in relation to the CS activity. Right, CS activity. Error bars indicate SD of three independent experiments. ***, $p < 0.001$ (Student's *t* test). (B) The absorbance spectra of different heme types were measured in mitochondria described in A. Heme C, B, and A are detected at wavelengths of 551, 561, and 603 nm, respectively.

We noticed that the absence of Coi1 results in defects in the assembly of complexes III and IV. Additionally, we detected heme only at the supercomplex level, suggesting that the affinity of the complex subunits to heme is probably higher when complex IV is part of a supercomplex. An additional explanation for this observation might be that, under the conditions occurring in mutant cells, which harbor low level of correctly assembled cytochrome *c* oxidase, all Cox complexes were immediately assembled into supercomplexes. This in turn might suggest that, in the mutant organelles, the heme association is the rate-limiting step for supercomplex formation. Taken together, deletion of Coi1 might lead to altered levels of complex III/IV or a dead-end assembly intermediate, and the absence of Coi1 can impair the final step of complex III assembly.

The clear reduction in the heme staining and heme A absorbance of complex IV raises the possibility that Coi1 facilitates, directly or indirectly, heme assembly to the complex. Heme A is required for the proper folding of Cox1, a core subunit of complex IV, and it also stabilizes the interaction between Cox1 and other subunits of complex IV (Kim *et al.*, 2012). Our results show a major reduction in the overall absorbance of heme A, suggesting a potential defect in synthesis or insertion of heme A.

The process that assures heme insertion into the mature Cox1 is not resolved yet. Cox1 is assembled cotranslationally (Friedman *et al.*, 2015) into the IM, and it forms a subcomplex with chaperones (Cox14, Cox25, and mitochondrial Hsp70), assembly factors (Coa1, Coa2, Coa3, and Shy1), and complex IV subunits (Cox5a and Cox6). At this stage, heme A seems to be incorporated in the vicinity of Shy1 (Mashkevich *et al.*, 1997; Kim *et al.*, 2012; Bareth *et al.*, 2013). One can speculate that Coi1 might be directly or indirectly involved in the incorporation of heme into mature Cox1. However, because mutating the potential heme-binding motif did not affect the functionality of Coi1, it seems that, if Coi1 is playing a role in heme assembly, this role does not involve a direct binding of Coi1 to a heme group.

Structure–function relationship of Coi1

Coi1 is anchored to the IM, probably via a TMS in its N-terminal region, and this segment is essential for the stability of the protein. Coi1 has no predicted canonical cleavable presequence, and the removal of its first nine amino acid residues did not alter its mitochondrial targeting. Thus Coi1 is most likely targeted to mitochondria by an internal targeting signal, which likely includes its TMS.

The hydrophilic C-terminal region of Coi1 has relatively low sequence conservation with other fungi but contains clusters of highly conserved positively charged amino acids. Variants truncated for these residues lost their activity but were still correctly embedded in the mitochondrial IM. Hence these positively charged residues are not involved in targeting and/or sorting of the protein but rather might play a structural role or are potentially involved in interactions with other proteins. One can even speculate that these residues might interact with the negatively charged head groups of the membrane phospholipids. Of note, truncation of the C-terminal region resulted in reduced binding to Cox2 or Cor1 but unaltered association with Cox4 or Mic60. Thus it seems that various regions in the protein are involved in interactions with different proteins.

The current study demonstrates that Coi1 interacts with elements of complexes III and IV that are composed from core subunits and accessory factors. The latter, which assist in the regulation, assembly, or stabilization of the respiratory complexes, are mostly small, contain a single TMS, and are nuclear encoded (Friedman *et al.*, 2015). In agreement with its suggested function, Coi1 shares these characteristics. Furthermore, the hydrophilic region of these subunits contains an unusually high percentage of charged residues. For example, around 50% of the residues in the C-terminal domains of the bovine ATP synthase e, f, and k subunits are charged ones (Friedman *et al.*, 2015; Unger *et al.*, 2017). Similarly, around 34% of Coi1's sequence is made up of charged residues. The lack of Coi1 homologues in higher eukaryotes is also not an unusual feature of the accessory factors. Collectively Coi1 shares several structural features with other accessory subunits of the respiratory complexes.

Potential functions of Coi1

Based on our results, the phenotype of the deletion of *COI1* could be explained by several options, which are depicted in Supplemental Figure S14 and are not mutually exclusive. Coi1 might have a function in assembling the supercomplexes formed between complexes III and IV. Lack of Coi1 clearly leads to a drastic reduction of complex IV activity and to a severe effect on the assembly of the III_2IV_2 supercomplex. Considering the physical interaction of

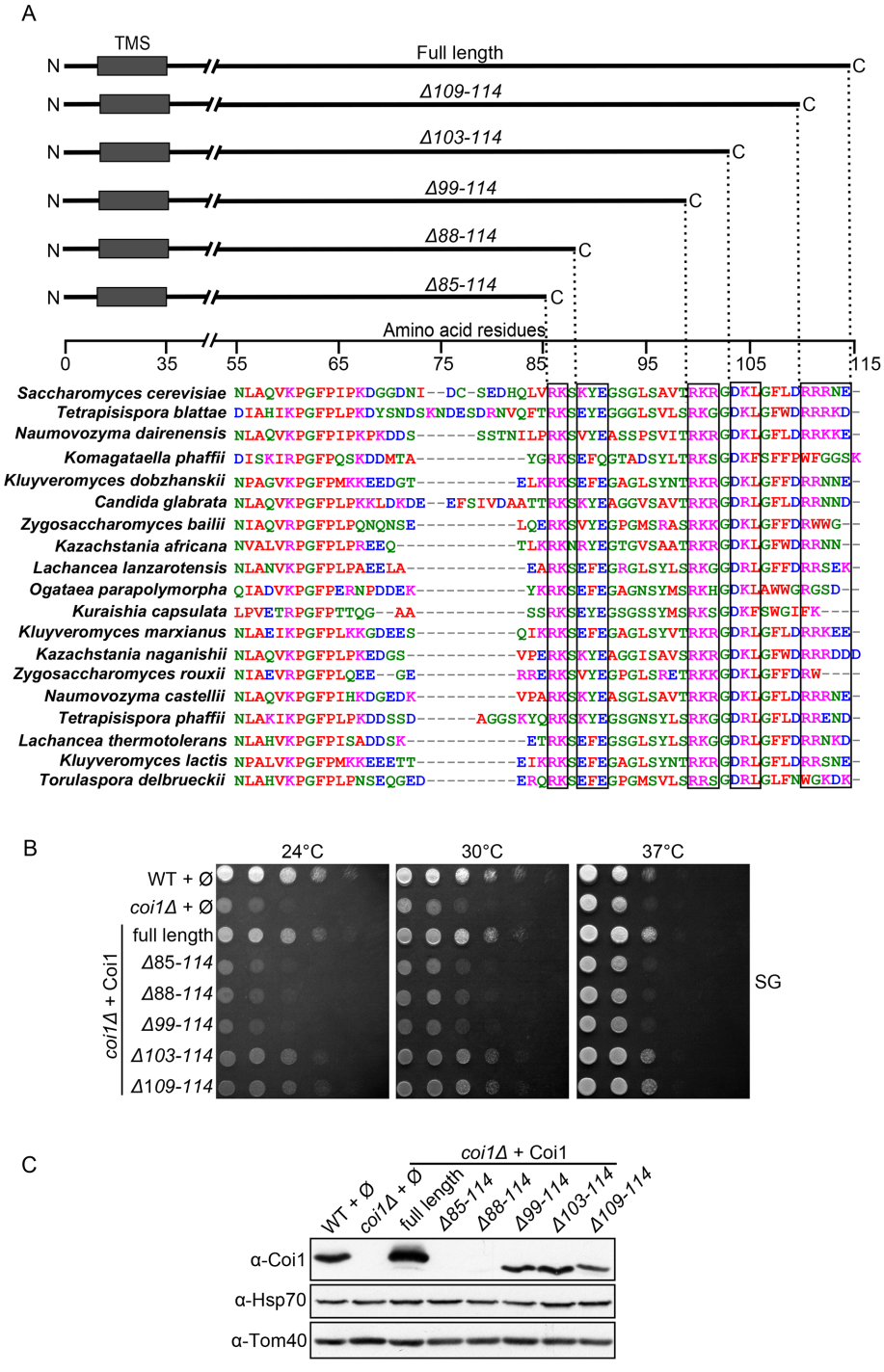

FIGURE 10: Conserved residues at the C-terminal region of Coi1 are required for its function. (A) Top, schematic representation of full-length and truncated versions of Coi1. Bottom, sequence similarity alignment by position-specific iterated BLAST of Coi1 in different fungi. (B) Wild-type (WT) or *coi1*Δ cells were transformed with an empty plasmid or with a plasmid encoding full-length or truncated versions of Coi1. The cells were subjected to a drop-dilution assay at the indicated temperatures on synthetic glycerol medium. (C) Crude mitochondria were isolated from the strains described in B. Samples were analyzed by SDS–PAGE and immunodecorated with the indicated antibodies. Antibodies against Coi1 were raised against a mixture of two peptides (peptide 1: aa 101–114; peptide 2: aa 83–96).

Coi1 with Rcf1, both proteins might act as an interface between complexes III and IV. Alternatively, Coi1 might also function as a modulator of the correct arrangement of complexes III and IV. A third option is that, in the absence of Coi1, heme A is not incorporated into the early Cox1-containing complex, and this is turn leads to a stalled intermediate complex. Furthermore, the growth retardation at low temperature on fermentable carbon source might suggest that Coi1 has an additional function beside its involvement in respiration. Regardless of the correct alternative, this study identifies Coi1 as a novel protein that is required for optimal function of mitochondria in yeast cells.

MATERIALS AND METHODS

Yeast strains and growth conditions

Standard genetic techniques were used for growth and manipulation of yeast strains. Yeast strains used in the study were isogenic to *Saccharomyces cerevisiae* strain W303a. For the deletion of *COI1* (*YDR381C-A*), PCR-mediated gene-specific replacement of the corresponding locus was performed employing homologous replacement by *HIS3*-MX6 cassette. Transformation of yeast cells was performed by the lithium acetate method. Deletion of *COI1* was confirmed by PCR with gene-specific primers.

Yeast cells were grown in standard rich medium YP (2% [wt/vol] bacto peptone, 1% [wt/vol] yeast extract), synthetic medium S (0.67% [wt/vol] bacto-yeast nitrogen base without amino acids) with glucose (2% [wt/vol], D), galactose (2% [wt/vol], Gal), sucrose (2% [wt/vol], Suc), or glycerol (3% [wt/vol], G) as carbon source or lactate medium (0.3% [wt/vol] yeast extract, 0.5 g/l glucose, 0.5 g/l NaCl, 1 g/l KH_2PO_4, 1 g/l NH_4Cl, 0.6 g/l $MgCl_2$, 0.5 g/l $CaCl_2$, 2% [vol/vol] lactic acid, pH 5.5). For drop-dilution assay, cells were grown in a synthetic medium to an OD_{600} of 1.0 or 2.0 and diluted in fivefold increments followed by spotting 5 µl of the diluted cells on solid media.

Recombinant DNA techniques

The ORF of *COI1* was amplified by PCR from *S. cerevisiae* genomic DNA with specific primers containing the restriction sites of *Eco*R1 and *Bam*H1 and cloned into the yeast shuttle centromeric plasmid pYX142 (*TPI* promoter). The *COI1* gene has an intron, which was excluded by PCR with gene-specific primers. The C-terminal HA-tagged *COI1* was obtained by cloning *COI1* without a stop codon into the pYX142 plasmid. The correct sequence of all constructs used was confirmed by DNA sequencing using specific primers.

Subcellular and submitochondrial fractionations

Subcellular fractionation was performed as described previously (Walther *et al.*, 2009). Isolation of mitochondria from yeast cells was performed by differential centrifugation. To obtain pure

mitochondria, a Percoll gradient in which mitochondria are layered on the top of the gradient was performed according to the published procedure (Graham, 2001). Sucrose gradient to separate OM and IM vesicles by centrifugation was performed as described previously (Tan *et al.*, 2013).

Microscopy

Electron microscopy of chemically fixed yeast cells was performed as previously described (Unger *et al.*, 2017). For visualization of mitochondria, yeast cells were transformed with an expression vector harboring the mitochondrial presequence of subunit 9 of Fo-ATPase of *Neurospora crassa* fused to GFP. Microscopy images were acquired with an Axioskop20 fluorescence microscope equipped with an Axiocam MRm camera using the 43 Cy3 filter set and AxioVision software (Zeiss).

Biochemical methods

Mitochondrial swelling was performed by resuspending the isolated organelles in hypotonic buffer (20 mM HEPES, pH 7.2), which was followed by incubation for 30 min on ice. The soluble fraction was precipitated with 12% trichloroacetic acid (TCA), whereas the mitoplasts were pelleted by centrifugation (30,000 × *g*, 20 min, 4°C). For the protease protection assay, mitochondria (50 µg) were resuspended in 100 µl of SEM buffer (250 mM sucrose, 1 mM EDTA, and 10 mM MOPS, pH 7.2). The samples were supplemented with PK (50 or 200 µg/ml) and incubated on ice for 30 min. As a control, mitochondria were treated with 0.2% Triton X-100 in SEM buffer on ice for 20 min and then subjected to PK treatment as described above. Next the samples were precipitated by TCA. To stop the proteolytic reaction, 2 µl of 200 mM phenylmethylsulfonyl fluoride (PMSF) was added to all samples. Mitochondria were reisolated (18,000 × *g*, 20 min, 2°C), and the pellet was resuspended in 50 µl of 2× Laemmli buffer, heated for 5 min at 95°C, and then analyzed by SDS–PAGE.

Rabbit reticulocyte lysate was used to synthesize precursor proteins radiolabeled with [^{35}S]methionine. The import of precursor proteins was performed in the presence of isolated mitochondria (50 µg) at 25°C for the indicated time periods in import buffer containing 250 mM sucrose, 0.25 mg/ml bovine serum albumin (BSA), 80 mM KCl, 5 mM $MgCl_2$, 10 mM MOPS-KOH, 2 mM NADH, and 2 mM ATP, pH 7.2. The import reactions were stopped by diluting the import reaction with SEMK^{80} buffer (250 mM sucrose, 80 mM KCl, 10 mM MOPS, and 1 mM EDTA, pH 7.2), and mitochondria were reisolated (12,000 × *g*, 2 min, 4°C). In some cases, the organelles were treated with PK as described above before their reisolation. The mitochondrial pellets were resuspended in 2× Laemmeli buffer and analyzed by SDS–PAGE. In some cases, samples were analyzed by BN-PAGE followed by autoradiography.

Western blotting

Protein samples were analyzed on 10–15% SDS–PAGE and subsequently transferred onto nitrocellulose membranes using a semi-dry Western blotting technique. For detection of proteins, primary antibodies were incubated with the membrane followed by peroxidase-conjugated goat anti-rabbit or goat anti-rat secondary antibodies. An antibody against Coi1 was raised in rabbit against a mixture of two peptides (peptide 1: aa 101–114 RGDKLGFLDRRRNE; peptide 2: aa 83–96 LVRKSKYE GSGLSA).

BN-PAGE

Isolated mitochondria (700 µg protein) were resuspended in 70 µl buffer A (50 mM NaCl, 50 mM imidazole, 2 mM aminocaproic acid, and 5 mM EDTA), solubilized by adding digitonin to a final concentration of 2.5% (wt/vol), and centrifuged (22,000 × *g*, 10 min, 4°C). The protein amount in the supernatant was determined, and samples of 50 µg were each supplemented with 0.75 µl of 5% Coomassie and 1.25 µl of 50% glycerol and analyzed on a 3–18% acrylamide gradient gel. BN gel electrophoresis was performed as described previously (Wittig *et al.*, 2006). Native gels were either blotted onto polyvinylidene fluoride membranes or fixed and stained with Coomassie. Then they were further processed for complexome profiling, exposed to autoradiography, immunodecorated with antibodies, or used for a cytochrome *c* oxidase heme-staining assay (Zerbetto *et al.*, 1997; Wittig *et al.*, 2007).

Oxygen-consumption measurements

Mitochondrial respiration of yeast cells was measured using high-resolution respirometry (Oxygrapgh-2k, Oroboros Instruments) with DatLab 6.1.0.7 software (Oroboros Instruments). Measurements were performed at 30°C with wild-type and *coi1*Δ cells grown on YPGal medium. Routine respiration was measured for 20 min followed by a stepwise addition of the uncoupler FCCP until maximal uncoupled respiration was reached. Residual oxygen consumption (ROX) was determined by azide inhibition of cytochrome *c* oxidase. Absolute respiration rates were corrected using ROX and normalized for total cell number.

Oxygen consumption of isolated mitochondria was measured at 25°C by resuspending organelles (100 µg) isolated from wild-type, *coi1*Δ, or *oxa1*Δ cells in 400 µl buffer containing 0.6 M sorbitol, 5 mM EDTA, and 20 mM HEPES/KOH (pH 7.4). The suspension was transferred into an electrode chamber of an oxygen measurement system (Oxygraph plus). After equilibration, 7.5 mM NADH was added, and the respiration-dependent consumption of oxygen was analyzed over time.

Mitochondrial membrane potential measurement

The membrane potential across the IM ($\Delta\Psi$) was measured by fluorescence quenching of the $\Delta\Psi$-sensitive dye $DiSC_3(5)$. A sample of the dye (3 µl of 2 µM in ethanol) was added at 25°C to a cuvette with 3 ml buffer containing 0.6 M sorbitol, 0.1% (wt/vol) BSA fatty acid–free, 0.5 mM EDTA, and 20 mM KPI (pH 7.2). Fluorescence was monitored with excitation at 622 nm and emission at 670 nm, and the data were taken at 2-s intervals. Once the fluorescence of the dye was stabilized, 50 µg of mitochondria in SEM buffer was added to the cuvette, and fluorescence was further measured until a stable signal was obtained. To completely dissipate the membrane potential, 3 µl of valinomycin (1 µM in ethanol) was added to the buffer, and the increase in the fluorescence was followed. For the assessment of the membrane potential, the difference between the fluorescence level before and after the addition of the valinomycin was estimated.

UV–visible spectroscopy of mitochondria

Detergent-solubilized mitochondria were divided into two samples (0.4 ml each), one oxidized by addition of 10 µl ferricyanide (200 mM) and the other reduced by addition of 10 µl of freshly prepared sodium dithionite solution (500 mM). The redox spectra of cytochromes (reduced minus oxidized sample) were recorded using a Shimadzu UV–VIS spectrophotometer UV-1800 between 530 and 630 nm.

In vivo and in organello labeling of mitochondrial translated proteins

For in vivo labeling of mitochondrially encoded proteins, wild-type and *coi1*Δ cells were grown to log phase (OD_{600} 0.3–0.6) in YP medium using either galactose or glucose as carbon source. Cells were harvested by centrifugation, resuspended in synthetic medium

lacking methionine, and treated with 150 µg/ml cycloheximide to block cytosolic translation. Radiolabeled [^{35}S]methionine was then added to the cell suspension to label mitochondrial proteins, and the samples were incubated at 30°C for various periods. To stop the reaction, an excess amount of cold methionine was added for 2 min before cellular proteins were extracted by alkaline solution and analyzed by SDS–PAGE and autoradiography.

The in organello labeling was performed as follows: isolated mitochondria (50 µl of 10 mg/ml) were mixed with 120 µl 1.5× ioTL buffer (375 µl 2.4 M sorbitol, 225 µl 1 M KCl, 22.5 µl 1 M KP_i, pH 7.2, 30 µl 1 M Tris/HCl, pH 7.2, 19 µl 1 M $MgSO_4$, 45 µl 100 mg/ml BSA [fatty acid–free], 9.1 µl 2 mg/ml of each amino acid except for methionine, cysteine, and tyrosine, 10 µl 10 mM cysteine, 18.2 µl 1 mg/ml tyrosine, 30 µl 200 mM ATP, 15 µl 50 mM GTP, 1.7 mg α-ketoglutarate, 3.5 mg phosphoenol pyruvate, 131.2 µl water, and 5 µl pyruvate kinase) and incubated for 2 min at 25°C. Then 5 µl [^{35}S] methionine was added to the sample to label the translation products for 30 min. Next 180 µl cold 0.2 M methionine was added, and after 5 min, mitochondria were pelleted for 10 min at 10,000 rpm, washed, and analyzed by two-dimensional BN-PAGE.

Pull-down assays

Isolated mitochondria (1 mg) were solubilized for 30 min at 4°C in 600 µl of lysis buffer (50 mM sodium phosphate, pH 7.5, 10 mM MOPS, 20% glycerol, 1× cocktail protease inhibitor, and 1 mM PMSF) containing 0.5% (wt/vol) Triton X-100. Anti-HA magnetic beads were washed twice with lysis buffer and equilibrated with lysis buffer for 30 min at 4°C. The solubilized organelles were subjected to a clarifying spin (30,000 × *g*, 20 min, 4°C), and the supernatant was incubated overnight at 4°C with the anti-HA beads. The unbound material was removed from the beads, and the beads were washed thoroughly with lysis buffer containing 0.1% Triton X-100. Bound proteins were eluted with sample buffer without reducing agent and analyzed by SDS–PAGE.

Sample preparation for MS

The anti-HA beads from the pull-down assays described above were resuspended in 20 µl of solution containing 6 M guanidine hydrochloride (GdmCl), 50 mM Tris/HCl (pH 8.5), and 10 mM Tris (2-carboxyethyl) phosphine and incubated at 95°C for 5 min. Reduced thiols were alkylated with 40 mM chloroacetamid, and samples were diluted with 25 mM Tris/HCl (pH 8.5) and 10% acetonitrile to obtain a final GdmCl concentration of 0.6 M. Proteins were digested overnight at 37°C under gentle agitation with 1 µg trypsin (sequencing grade, Promega). Digestion was stopped by adding trifluoroacetic acid to a final concentration of 0.5%. Peptides were loaded on a multi-stop-and-go tip (StageTip) containing six C18 disks (Rappsilber *et al.*, 2007). Peptides were eluted in wells of microtiter plates, dried, and resolved in 1% acetonitrile and 0.1% formic acid.

Sample preparation for complexome profiling

Each lane of the BN-PAGE was cut into 50 equal fractions and collected in 96-well filter plates (30–40 µm PP/PE; Pall Corporation). The gel pieces were destained in 60% methanol and 50 mM ammonium bicarbonate (ABC). Solutions were removed by centrifugation (600 × *g*, 2 min). Proteins were then reduced at 56°C for 1 h in 10 mM dithiothreitol and 50 mM ABC and alkylated for 45 min in 30 mM iodoacetamid. Samples were digested for 16 h with trypsin (sequencing grade) at 37°C in 50 mM ABC, 0.01% Protease Max (Promega), and 1 mM $CaCl_2$. Peptides were eluted in 30% acetonitrile and 3% formic acid, centrifuged into a fresh 96-well plate, dried in a speed vacuum, and resolved in 1% acetonitrile and 0.5% formic acid.

Liquid chromatography/MS

Liquid chromatography/MS (LC/MS) was performed on a Thermo Scientific Q Exactive Plus equipped with an ultra–high performance LC unit (Thermo Scientific Dionex Ultimate 3000) and a Nanospray Flex Ion-Source (Thermo Scientific). Peptides were loaded on a C18 reverse-phase precolumn (Thermo Scientific); this was followed by separation on a 2.4 µm Reprosil C18 resin (Dr. Maisch GmbH) in-house–packed picotip emitter tip (100 µm diameter, 30 cm length; New Objectives). A gradient from mobile phase A (4% acetonitrile, 0.1% formic acid) to 40% of mobile phase B (80% acetonitrile, 0.1% formic acid) for 60 min was used, followed by a second gradient to 80% of mobile phase B for 30 min with a flow rate of 400 nl/min. The gradient for complexome profiling was for 30 min until 60% of mobile phase B was reached.

MS data were recorded by a data-dependent acquisition top 10 method selecting the most abundant precursor ions in positive mode for higher-energy collisional dissociation fragmentation. Lock mass option was enabled to ensure high mass accuracy during many following runs (Olsen *et al.*, 2005). The full MS scan range was 300–2000 *m/z* with resolution of 70,000 and an automatic gain control (AGC) value of 3×10^6 total ion counts with a maximal ion-injection time of 160 ms. MS/MS scans were recorded with a resolution of 17,500, an isolation window of 2 *m/z*, and an AGC value set to 10^5 ions with a maximal ion-injection time of 150 ms. Selected ions were excluded in a time frame of 20 s following the fragmentation event. Full-scan data were acquired in profile, and fragments were analyzed in centroid mode by Xcalibur software. The LC unit was controlled by Chromeleon Xpress software.

MS data analysis

For data analysis, MaxQuant 1.5.3.30 (Cox and Mann, 2008), Perseus 1.5.4.1 (Tyanova *et al.*, 2016), and Excel (Microsoft Office 2013) were used. The enzyme specificity was set to trypsin, and missed cleavages were limited to 2. N-terminal acetylation (+42.01) and oxidation of methionine (+15.99) were selected as variable modifications, and carbamidomethylation (+57.02) on cysteines was selected as a fixed modification. The *S. cerevisiae* reference proteome set (Uniprot, March 2016) was used to identify peptides and proteins with a false discovery rate (FDR) less than 1%. The minimal ratio count for label-free quantification (LFQ) was 1. Reverse identifications and common contaminants were removed, and the data set was reduced to proteins that were identified in at least four of six samples in one experimental group. LFQ values were normalized to median, and missing values were replaced by random background values. Significantly interacting proteins were determined by permutation-based FDR calculation. Proteins were plotted in a volcano plot, setting threshold for proteins of interest at FDR <0.03. For complexome profiling, intensity-based absolute quantification (IBAQ) values were used to generate abundance profiles of proteins as described in Strecker *et al.* 2016.

ACKNOWLEDGMENTS

We thank Elena Kracker, Sara Bernhard, Rita Grotjahn, and Jana Meisterknecht for excellent technical assistance; Andreas Reichert for strains and antibodies; and Kai S. Dimmer for helpful discussions. This work was supported by the Deutsche Forschungsgemeinschaft (SFB 815 project Z01 to I.W., RA 1028/7-1 to D.R., and DIP to J.H. and D.R.), the German-Israeli Foundation (GIF I-1190-96.13/2012 to D.R.), and the International Max Planck Research School "From Molecules to Organisms" (to R.K.S.).

REFERENCES

Allen JW, Ginger ML, Ferguson SJ (2004). Maturation of the unusual single-cysteine (XXXCH) mitochondrial c-type cytochromes found in trypanosomatids must occur through a novel biogenesis pathway. Biochem J 383, 537–542.

Bareth B, Dennerlein S, Mick DU, Nikolov M, Urlaub H, Rehling P (2013). The heme a synthase Cox15 associates with cytochrome *c* oxidase assembly intermediates during Cox1 maturation. Mol Cell Biol 33, 4128–4137.

Barrientos A, Gouget K, Horn D, Soto IC, Fontanesi F (2009). Suppression mechanisms of COX assembly defects in yeast and human: insights into the COX assembly process. Biochim Biophys Acta 1793, 97–107.

Bottinger L, Guiard B, Oeljeklaus S, Kulawiak B, Zufall N, Wiedemann N, Warscheid B, van der Laan M, Becker T (2013). A complex of Cox4 and mitochondrial Hsp70 plays an important role in the assembly of the cytochrome *c* oxidase. Mol Biol Cell 24, 2609–2619.

Cogliati S, Frezza C, Soriano ME, Varanita T, Quintana-Cabrera R, Corrado M, Cipolat S, Costa V, Casarin A, Gomes LC, *et al*. (2013). Mitochondrial cristae shape determines respiratory chain supercomplexes assembly and respiratory efficiency. Cell 155, 160–171.

Cox J, Mann M (2008). MaxQuant enables high peptide identification rates, individualized p.p.b.-range mass accuracies and proteome-wide protein quantification. Nat Biotechnol 26, 1367–1372.

Cruciat CM, Brunner S, Baumann F, Neupert W, Stuart RA (2000). The cytochrome bc_1 and cytochrome *c* oxidase complexes associate to form a single supracomplex in yeast mitochondria. J Biol Chem 275, 18093–18098.

Friedman JR, Mourier A, Yamada J, McCaffery JM, Nunnari J (2015). MICOS coordinates with respiratory complexes and lipids to establish mitochondrial inner membrane architecture. eLife 4, e07739.

Geier BM, Schägger H, Ortwein C, Link TA, Hagen WR, Brandt U, Von Jagow G (1995). Kinetic properties and ligand binding of the eleven-subunit cytochrome-*c* oxidase from *Saccharomyces cerevisiae* isolated with a novel large-scale purification method. Eur J Biochem 227, 296–302.

Genova ML, Lenaz G (2014). Functional role of mitochondrial respiratory supercomplexes. Biochim Biophys Acta 1837, 427–443.

Graham JM (2001). Purification of a crude mitochondrial fraction by density-gradient centrifugation. Curr Protoc Cell Biol Chap 3, Unit 3.4.

Greggio C, Jha P, Kulkarni SS, Lagarrigue S, Broskey NT, Boutant M, Wang X, Conde Alonso S, Ofori E, Auwerx J, *et al*. (2017). Enhanced respiratory chain supercomplex formation in response to exercise in human skeletal muscle. Cell Metabolism 25, 301–311.

Heinemeyer J, Braun H-P, Boekema EJ, Kouril R (2007). A structural model of the cytochrome *c* reductase/oxidase supercomplex from yeast mitochondria. J Biol Chem 282, 12240–12248.

Herrmann JM, Woellhaf MW, Bonnefoy N (2013). Control of protein synthesis in yeast mitochondria: the concept of translational activators. Biochim Biophys Acta 1833, 286–294.

Horn D, Barrientos A (2008). Mitochondrial copper metabolism and delivery to cytochrome *c* oxidase. IUBMB Life 60, 421–429.

Kim HJ, Khalimonchuk O, Smith PM, Winge DR (2012). Structure, function, and assembly of heme centers in mitochondrial respiratory complexes. Biochim Biophys Acta 1823, 1604–1616.

Levchenko M, Wuttke JM, Rompler K, Schmidt B, Neifer K, Juris L, Wissel M, Rehling P, Deckers M (2016). Cox26 is a novel stoichiometric subunit of the yeast cytochrome *c* oxidase. Biochim Biophys Acta 1863, 1624–1632.

Mashkevich G, Repetto B, Glerum DM, Jin C, Tzagoloff A (1997). SHY1, the yeast homolog of the mammalian SURF-1 gene, encodes a mitochondrial protein required for respiration. J Biol Chem 272, 14356–14364.

Mavridou DA, Stevens JM, Monkemeyer L, Daltrop O, di Gleria K, Kessler BM, Ferguson SJ, Allen JW (2012). A pivotal heme-transfer reaction intermediate in cytochrome *c* biogenesis. J Biol Chem 287, 2342–2352.

Mick DU, Fox TD, Rehling P (2011). Inventory control: cytochrome *c* oxidase assembly regulates mitochondrial translation. Nat Rev Mol Cell Biol 12, 14–20.

Olsen JV, de Godoy LM, Li G, Macek B, Mortensen P, Pesch R, Makarov A, Lange O, Horning S, Mann M (2005). Parts per million mass accuracy on an Orbitrap mass spectrometer via lock mass injection into a C-trap. Mol Cell Proteomics 4, 2010–2021.

Pfeiffer K, Gohil V, Stuart RA, Hunte C, Brandt U, Greenberg ML, Schägger H (2003). Cardiolipin stabilizes respiratory chain supercomplexes. J Biol Chem 278, 52873–52880.

Rappsilber J, Mann M, Ishihama Y (2007). Protocol for micro-purification, enrichment, pre-fractionation and storage of peptides for proteomics using StageTips. Nat Protoc 2, 1896–1906.

Rydstrom Lundin C, von Ballmoos C, Ott M, Adelroth P, Brzezinski P (2016). Regulatory role of the respiratory supercomplex factors in *Saccharomyces cerevisiae*. Proc Natl Acad Sci USA 113, E4476–E4485.

Schägger H, Pfeiffer K (2000). Supercomplexes in the respiratory chains of yeast and mammalian mitochondria. EMBO J 19, 1777–1783.

Smith PM, Fox JL, Winge DR (2012). Biogenesis of the cytochrome bc_1 complex and role of assembly factors. Biochim Biophys Acta 1817, 276–286.

Soto IC, Fontanesi F, Liu J, Barrientos A (2012). Biogenesis and assembly of eukaryotic cytochrome *c* oxidase catalytic core. Biochim Biophys Acta 1817, 883–897.

Strecker V, Kadeer Z, Heidler J, Cruciat CM, Angerer H, Giese H, Pfeiffer K, Stuart RA, Wittig I (2016). Supercomplex-associated Cox26 protein binds to cytochrome *c* oxidase. Biochim Biophys Acta 1863, 1643–1652.

Strogolova V, Furness A, Robb-McGrath M, Garlich J, Stuart RA (2012). Rcf1 and Rcf2, members of the hypoxia-induced gene 1 protein family, are critical components of the mitochondrial cytochrome bc_1-cytochrome *c* oxidase supercomplex. Mol Cell Biol 32, 1363–1373.

Tan T, Ozbalci C, Brügger B, Rapaport D, Dimmer KS (2013). Mcp1 and Mcp2, two novel proteins involved in mitochondrial lipid homeostasis. J Cell Sci 126, 3563–3574.

Tyanova S, Temu T, Sinitcyn P, Carlson A, Hein MY, Geiger T, Mann M, Cox J (2016). The Perseus computational platform for comprehensive analysis of (prote)omics data. Nat Methods 13, 731–740.

Unger AK, Geimer S, Harner M, Neupert W, Westermann B (2017). Analysis of yeast mitochondria by electron microscopy. Methods Mol Biol 1567, 293–314.

Walther DM, Papic D, Bos MP, Tommassen J, Rapaport D (2009). Signals in bacterial beta-barrel proteins are functional in eukaryotic cells for targeting to and assembly in mitochondria. Proc Natl Acad Sci USA 106, 2531–2536.

Wittig I, Braun H-P, Schägger H (2006). Blue native PAGE. Nat Protoc 1, 418–428.

Wittig I, Karas M, Schägger H (2007). High resolution clear native electrophoresis for in-gel functional assays and fluorescence studies of membrane protein complexes. Mol Cell Proteomics 6, 1215–1225.

Zahedi RP, Sickmann A, Boehm AM, Winkler C, Zufall N, Schönfisch B, Guiard B, Pfanner N, Meisinger C (2006). Proteomic analysis of the yeast mitochondrial outer membrane reveals accumulation of a subclass of preproteins. Mol Biol Cell 17, 1436–1450.

Zerbetto E, Vergani L, Dabbeni-Sala F (1997). Quantification of muscle mitochondrial oxidative phosphorylation enzymes via histochemical staining of blue native polyacrylamide gels. Electrophoresis 18, 2059–2064.